Optimization of the TEM Feed Structure for Four-Arm Reflector Impulse Radiating Antennas

J. Scott Tyo, *Member, IEEE*

***Abstract*—This paper considers the optimization of the feed arm geometry of four-arm crossed-coplanar plate impulse radiating antennas (IRAs) when the angular position and extent of the arms are taken as free parameters. Previously, optimization of this class of antenna considered only the symmetric case where the two pairs of crossed feed arms were perpendicular to each other. Comparison is made using the prompt aperture efficiency, and the results indicate that the efficiency of four-arm IRAs can be increased from ∼25% for the perpendicularly crossed arms to ∼35% for the optimum configuration. In addition to the optimization, the feed impedance of coplanar feeds is presented for general values of feed arm angle and plate width, and the optimum feed impedance is computed for each feed arm angle. The results can be used to design the optimal four-arm IRA with an arbitrary specified input impedance.**

***Index Terms*—Reflector antennas, ultra-wide-band (UWB) antennas.**

I. Introduction

IMPULSE radiating antennas (IRAs) are members of a class of antennas that are designed for the radiation of ultra-wide-band (UWB) electromagnetic impulses. These antennas are perhaps better characterized as dispersionless high-band ratio antennas, where band ratio is defined as the ratio of the upper and lower 3-dB rolloff frequencies of the radiated pulse. Current systems can achieve band ratios approaching 100 (two decades of instantaneous bandwidth) [1]. Through a combination of a nondispersive transverse electromagnetic (TEM) feed structure and a focused aperture, IRAs act like differentiators for the early time portion of the applied voltage waveform. When excited by a fast-rising step, the field radiated form the IRA on boresight closely resembles a narrow impulse. While the nature of the focusing optic and the feed structure affect the features of the prepulse and postpulse portions of the waveform, the largest part of the radiated signal for a general IRA is [2]–[6]

$$\mathbf{E}_{\mathrm{rad}}(r,t) = \frac{\iint_{S_a} \mathbf{E}(x,y)\,dx\,dy}{V_0 2\pi r c}\,\frac{dV(t)}{dt} \tag{1}$$

where $V(t)$ is the applied voltage waveform, V_0 is the peak of the applied voltage waveform, and the surface integral is over the transverse components of the TEM mode in the aperture defined by S_a. The prompt radiated field can also be described in terms of the geometric impedance factor of the TEM transmission line feed

$$f_g = Z_{\mathrm{line}}/Z_{\mathrm{med}} \tag{2}$$

and the aperture height [7]

$$h_a = -\frac{f_g}{V_0}\iint_{S_a} \mathbf{E}(x,y)\,dx\,dy. \tag{3}$$

The aperture height is a convenient parameter because both the transmitted and received peak waveforms can be expressed in terms of h_a as [3]

$$\begin{aligned} E_{\mathrm{rad}}(t) &= -\frac{h_a}{2\pi r c f_g}\,\frac{dV}{dt} \\ V_{\mathrm{rec}}(t) &= -h_a E_{\mathrm{inc}}(t) \end{aligned} \tag{4}$$

where E_{rad} and E_{inc} are the magnitudes of the principal component of the radiated and incident field, respectively.

A. Performance Metrics

A number of metrics have been proposed to compare the performance of antennas operating in the time domain [3], [8]–[10]. The difficulty in comparing performance arises from the nonunique choice of a norm for time-domain comparisons. The three metrics discussed below are the power normalized gain and voltage normalized gain introduced by Farr and Baum [3], [9] and the prompt aperture efficiency introduced by Buchenauer *et al.* [10], all of which make comparisons based on the peak radiated power or field.

The power normalized gain is defined as [9]

$$G_p = h_a/\sqrt{f_g} \tag{5}$$

and is useful for comparing the performance of antennas under constant input power conditions. When the input power is held constant ($V_0/\sqrt{f_g}$ constant), the response of an IRA is proportional to G_p. The voltage normalized gain is defined as [3], [9]

$$G_v = h_a/f_g \tag{6}$$

and is used for comparing the performance of antennas under constant input voltage conditions, i.e, when V_0 is held constant. For high-power applications, spark-gap sources have been developed that can provide a constant input voltage to an IRA, regardless of the feed impedance. In these cases, G_v is a useful metric. As shown in [9] and found below, G_v is often maximized by allowing the feed impedance to go to zero, an impractical scenario that requires infinite input power and results in

Manuscript received November 10, 1999; revised April 11, 2000. This work was supported in part by the Air Force Research Laboratory, Directed Energy Directorate, under the Air Force Office of Scientific Research New World Vistas Program and in part by the Naval Postgraduate School Merit Program.

The author is with the Department of Electrical and Computer Engineering, U.S. Naval Postgraduate School, Monterey, CA 93943 USA (e-mail: tyo@ieee.org).

Publisher Item Identifier S 0018-926X(01)01832-4.

0018–926X/01$10.00 © 2001 IEEE

infinite fields in the aperture and infinite currents on the electrodes. In these situations, other considerations such as source lifetime, maximum fields on the antenna and current flow limit the allowed values of f_g (and hence G_v).

The power normalized gain G_p has units of length, and care must be taken when using it in an optimization problem in order to make a fair comparison between antennas of different sizes, as G_p can be increased simply by increasing the physical size of the antenna. G_p is most useful when additional constraints are present that limit the dimensions of the antenna. For example, when optimizing the feed impedance of lens IRAs constrained to fit within a circular aperture of fixed radius, Farr and Baum [4], [11] used G_p to conclude that low-impedance horns (with large width to height ratios) were undesirable. This result is dominated by the fact that the physical height and aperture area of low-impedance horns that fit inside a circle of fixed radius goes to zero as $Z \to 0$.

The dimensionless quantity of prompt aperture efficiency is defined as [10]

$$\eta_a = \frac{1}{A} f_g \left[\frac{1}{V} \iint_{S_a} E_y(x,y)\, dx\, dy \right]^2 \tag{7}$$

where A is the area of the aperture defined by S_a and E_y is the principle component of the electric field in the aperture, taken without loss of generality as being parallel to the y-axis. Equation (7) is obtained by comparing the peak radiated power density boresight from an antenna to that from an ideal antenna with a uniformly illuminated aperture, the same input power, and the same aperture area. Because of the area normalization in (7), aperture efficiency is the preferred metric for comparing the inherent performance of classes antennas regardless of physical size. Aperture efficiency and power normalized gain are related by

$$\eta_a = G_p^2 / A. \tag{8}$$

Regardless of the metric, it is clear from (4)–(7) that the optimum antenna for a fixed input impedance (fixed f_g) and aperture size is the one that maximizes the aperture height h_a.

B. Self-Reciprocal Apertures

An important class of IRAs is the set of antennas fed by self-reciprocal feed structures. Self-reciprocal apertures are discussed in [12] and have feed geometries that are unaltered by the reciprocation operation $r \to a^2/r$, where $\mathbf{r} = r\cos\theta\hat{\mathbf{x}} + r\sin\theta\hat{\mathbf{y}}$ is the position vector in the aperture plane and a is the radius of the circle of symmetry. The coplanar feed IRAs discussed in this paper are examples of self-reciprocal apertures, as shown in Fig. 1. Self-reciprocal apertures have a number of interesting properties, but the most important ones for this paper are:

1) exactly half of the power on the transmission line propagates outside the circle of symmetry;
2) the total charge on the feed arms inside and outside the circle of symmetry are equal;
3) all contiguous points on the circle of symmetry that are not occupied by conductor lie on a single field line.

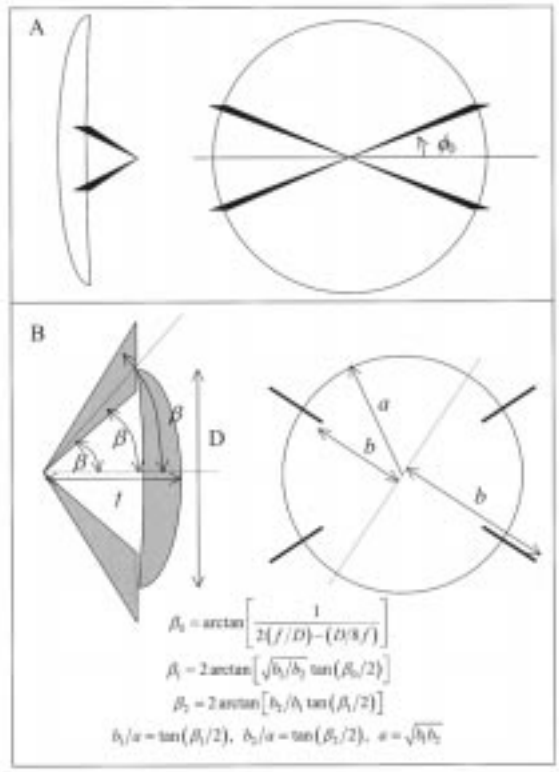

Fig. 1. Schematic of the arbitrary crossed coplanar feeds. The feed arms originate from the focal point of the paraboloidal reflector, and the plane of the feed arm makes an angle ϕ_0 with the horizontal symmetry plane. Each pair of feeds is taken to be coplanar, and the intersection point with the circle of symmetry (after sterographic projection) satisfies the self-reciprocal condition [1], [12]. Once the focal length f, diameter D, and ϕ_0 are specified and the ratio b_1/b_2 is chosen (equivalent to specifying feed impedance), β_0, β_1, and β_2 can be determined using the relations in the figure.

For the important class of self-reciprocal apertures, which are typically confined to focusing the fields within the circle of symmetry, the aperture area A is constant for all configurations, and η_a and G_p are equivalent metrics. Aperture efficiency will be the parameter used in this paper to optimize the feed configuration in crossed coplanar fed IRAs, primarily because of its dimensionless property and ready interpretation, but use of either η_A or G_p produces identical results for this class of IRAs.

C. Reflector IRAs with Crossed Coplanar Feeds

One of the most common types of IRAs used is the reflector IRA with two pairs of perpendicularly crossed, coplanar feeds [1] ($\phi_0 = 45°$ in Fig. 1). Because of the symmetry of the system, the field distribution, feed impedance, and aperture height of this type of antenna can be calculated analytically [2]. While there is no additional complexity associated with making a more general IRA with feed arms that are not oriented at right angles, the only analysis of crossed coplanar-fed IRAs whose arms make an arbitrary angle ϕ_0 with respect to the ground plane as shown in Fig. 1 was performed by Baum [13] for the high-impedance limit of wire-fed IRAs. In Section II, the TEM mode for the arbitrary coplanar, four-arm structure is computed numerically using the finite-element method. In Section III, the important design parameters of feed impedance, aperture height, and aperture efficiency are calculated. Section IV contains a discussion

of the results and implications of optimizing various features of the antenna. Conclusions are drawn in Section V.

II. Computation of the TEM Mode Distribution

It is well known that the field distribution of the TEM mode on a multiconductor transmission line can be computed as the gradient of a scalar potential that satisfies the Laplace equation [14]. For many classes of feeds, the potential can be calculated using a combination of the stereographic projection and conformal transformations [15]; however, for arbitrary geometries, the conformal map may not exist in closed form. In this paper, it is assumed that the stereographic projection has already been carried out, i.e., the conically symmetric feed structure has been transformed to a longitudinally symmetric structure, as discussed in [5]. The important properties of the stereographic projection for this class of antennas are summarized in Fig. 1 and discussed in greater detail in [5].

The asymmetrically crossed coplanar feed structure depicted in Fig. 1 can be described in terms of successive conformal mappings, but the Schwartz–Christoffel transformation integrals for the asymmetric cases ($\phi_0 \neq 45°$) have not been performed analytically. When the analytic form of the conformal transformation is not known, a numerical approximation can be obtained by employing a Laplace equation solver such as the method of moments or finite-element method (FEM). The properties of self-reciprocal symmetry allow the computational domain to be bounded, making the geometry depicted in Fig. 1 ideally suited to analysis by the FEM. After numerical calculation of the fields, the integrals in (1)–(7) can be evaluated directly or by casting the aperture integral into one of the alternate contour integral forms presented in [7].

The FEM requires a closed computational domain, so it is not always straightforward to calculate open-mode problems using FEM. The complex potential distribution on a TEM transmission line is an example of an open mode problem (because the TEM mode exists everywhere in the plane transverse to propagation), but the reflection symmetries at the $x = 0$ and $y = 0$ planes and the reciprocation symmetry on the circle of radius a shown in Fig. 1 allow the geometry to be bounded by perfectly electrically conducting (PEC) ($x = 0$) and perfectly magnetically conducting (PMC) ($x = 0; r = a$) surfaces. The symmetry planes also allow the structure to be modeled by considering only one quadrant of the antenna.

The FEM was employed in this study using the Matlab (version 5.3) Partial Differential Equations (PDE) Toolbox (version 1.0), which was designed to solve two-dimensional vector and scalar differential equations using the FEM. The electrode was positioned at an arbitrary position ϕ_0 from the x-axis and held at constant electric potential. The PDE toolbox required the electrode to have finite thickness, and past experience has shown that when the ratio of plate thickness to the next smallest dimension (either separation or width) was less than 1:60, the field distribution was very close to the theoretical zero-thickness plate result [10], [16]. The FEM mesh was composed of linear, triangular elements and was generated automatically by the PDE toolbox. After computation of a solution to the Laplace equation, the mesh was adaptively refined by subdividing elements where the gradient varied most rapidly in order to better approximate the local electric field near the plate edges.

A. Validation of Modeling Method

When $\phi_0 = 45°$, the two crossed pairs of coplanar feeds are perpendicular to each other, and the presence of the second set of electrodes does not alter the fields that are due to the first set alone. For a single pair of electrodes, the complex potential is given by the conformal transformation

$$\begin{aligned} z(w) &= jm^{1/4}\mathrm{sn}(w\,|\,m) \\ z &= x + iy; \quad w = u + iv \end{aligned} \tag{9}$$

where $\mathrm{sn}(w|m)$ is a Jacobian elliptic function [17] and m is the parameter of the elliptic function. In (9), u gives the electric potential and v gives the magnetic potential (or electric field lines). The product of the short and long radii of the electrode is fixed by the self-reciprocal symmetry condition to be $b_1 b_2 = a^2$, and the parameter of the elliptic function is given as $m = (b_1/b_2)^2$ [12]. The field distribution can be computed analytically by superposing the fields given by (9) for the two sets of feed arms taken one at a time [2], [3]. The feed impedance and aperture heights of the 4-arm IRA are [9]

$$f_g = \frac{K(m)}{2K(1-m)} \tag{10}$$

$$h_a = \frac{\pi m^{-1/4}}{2\sqrt{2}K(1-m)}\left[1 - \frac{2}{\pi}\arcsin\left(\frac{\left(1-m^{1/2}\right)^2}{1-m}\right)\right]. \tag{11}$$

This case can be used as a validation tool for the FEM modeling method. Furthermore, the performance of the adaptive mesh refinement described above can be evaluated, and a stopping criterion can be established for the general case where the analytic solution is not known.

The results of the numerical calculations of the feed impedance for the case of $\phi_0 = 45°$, $b_1/a = 0.5$ are shown in Fig. 2. The diagnostic quantity that was used for the stopping condition in the following sections was the geometric impedance factor f_g. The difference between the calculated value for f_g and the theoretical value ($f_g = 0.285$) as a function of iteration number is shown in Fig. 2(a), and the number of elements as a function of iteration number is shown in Fig. 2(b). The fractional change in the calculated f_g is shown as a function of iteration number in Fig. 2(c). As can be seen from the figure, the model can get to within ~1% of the theoretical value with a mesh size of ~5000 elements, a number that was fairly typical for most geometries (highly singular geometries where ϕ_0 was close to 0° or 90° or when b_1/a is close to one or zero required more highly refined meshes). Comparing the results presented in Fig. 2(a) and (c) led to the development of the following stopping criteria for the adaptive refinements: when three successive mesh refinements had a fractional change of less than 0.003 in the geometric impedance factor, the algorithm terminated. If the number of

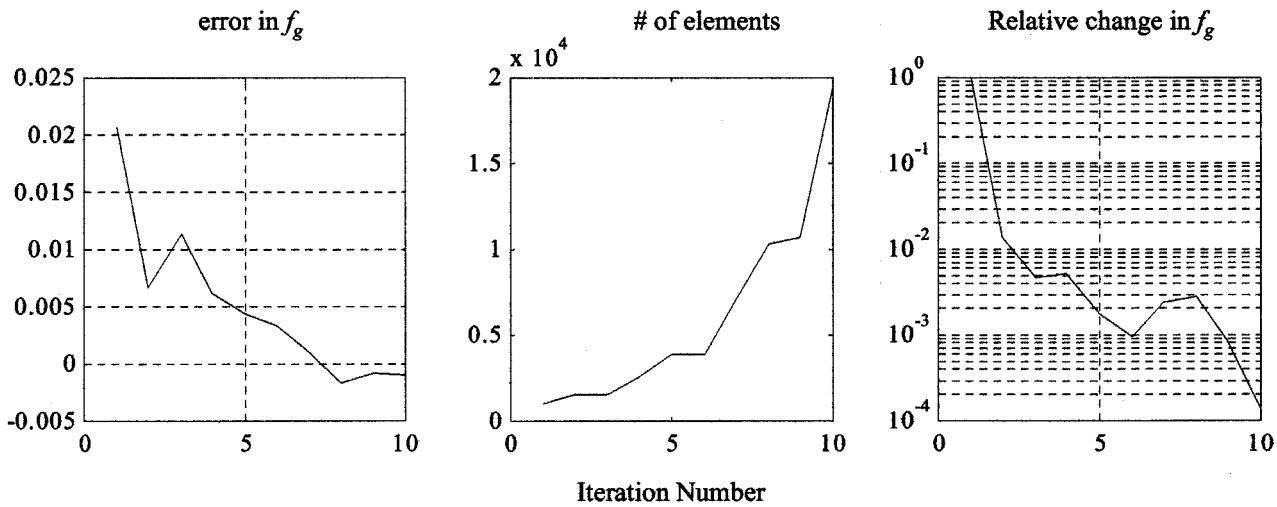

(a) (b) (c)

Fig. 2. Performance of the FEM modeling tool for the case of $\phi_0 = 45°$ and $b_1/a = 0.5$. The analytic solution for this case is known and $f_g = 0.285$. (a) Absolute error in the computed value of f_g as a function of iteration number. (b) Number of elements in FEM mesh. (c) Relative change in the computed value of f_g as a function of iteration number. These data were used to develop the stopping criterion discussed in the text.

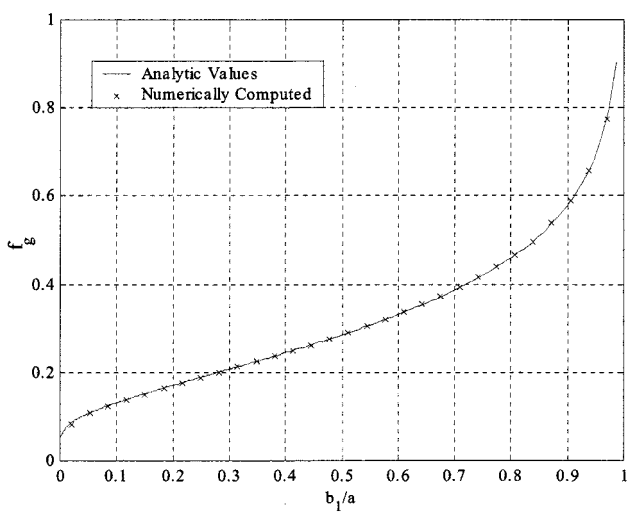

Fig. 3. Comparison of numerical computation of geometric impedance factor to the theoretical value predicted by (10). The fit is very close except for the first point $(b_1/a = 0.02)$, where the error is 2.1%. For all other points, the error is less that 0.5%.

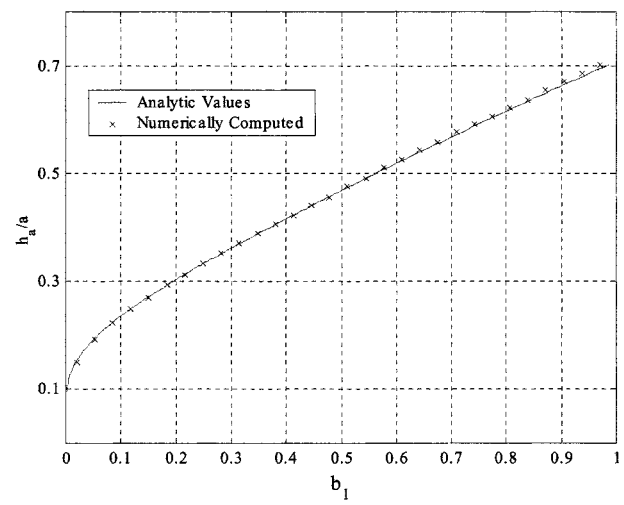

Fig. 4. Comparison of numerically computed values of aperture height to the theoretical values predicted by (11). The fit for aperture height is not as good as for the impedance; however, the error is less than 1.5% for all points except for the first $(b_1/a = 0.02)$.

elements in the mesh exceeded 7500, the adaptive refinement was also stopped regardless of the fractionalchange in f_g.

Fig. 3 presents a comparison of the computed and theoretical values of f_g for $\phi_0 = 45°$ over the range of b_1/a from 0.02 to 0.97. Theoretical values were obtained using (10). The computed values were taken from calculations employing the automatic stopping condition described above (not from the data that went into Fig. 2). Except at the lowest impedance $(b_1 = 0.02)$, the error between the calculated and analytic impedance values was less than 0.5%. At the lowest impedance, the error was 2.1%. Fig. 4 presents a comparison between the computed and analytic value for the aperture height. Analytic values were obtained using (11). The error at the lowest impedance was 2.1%, but for all other points the error was 1.2% or less.

III. Calculation of Antenna Design Parameters

Using the FEM method described in the previous section, the feed impedance, aperture height, and aperture efficiency were calculated at values of ϕ_0 ranging from 3° to 87° and at values of b_1/a ranging from 0.02 to 0.97.

A. Feed Impedance

Fig. 5 presents the value of b_1/a as a function of ϕ_0 to achieve popular values of the feed impedance. As expected, $Z_{\text{line}} \to 0$ as $b_1 \to 0$ (limit as the spacing between the electrodes goes to zero) and $Z_{\text{line}} \to \infty$ as $b_1/a \to 1$ (limit as the electrodes approach infinitesimal wires). The family of curves in Fig. 5 has been fitted to a functional form as described and tabulated in [18]. Appropriate values of b_1/a for a particular feed impedance

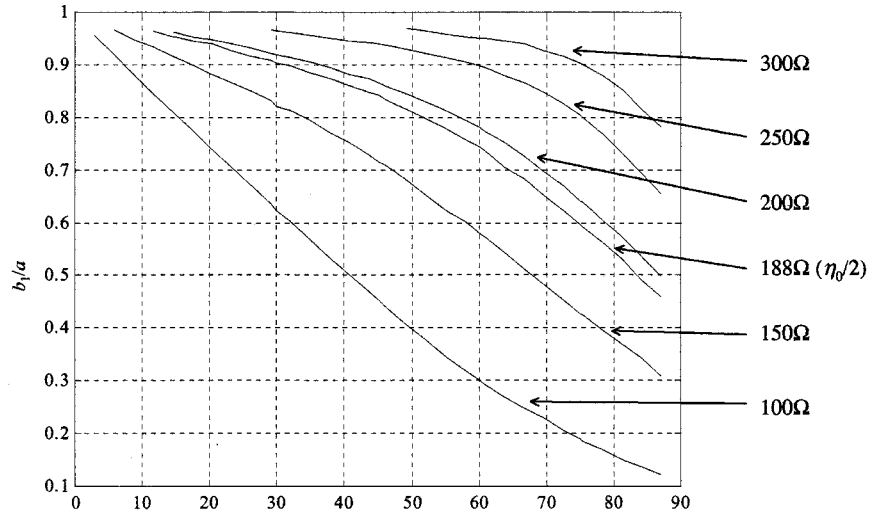

Fig. 5. Plate widths as a function of ϕ_0 to obtain popular values of feed impedance. To find the corresponding angular widths for the feed arms of an IRA, use the relations in Fig. 1.

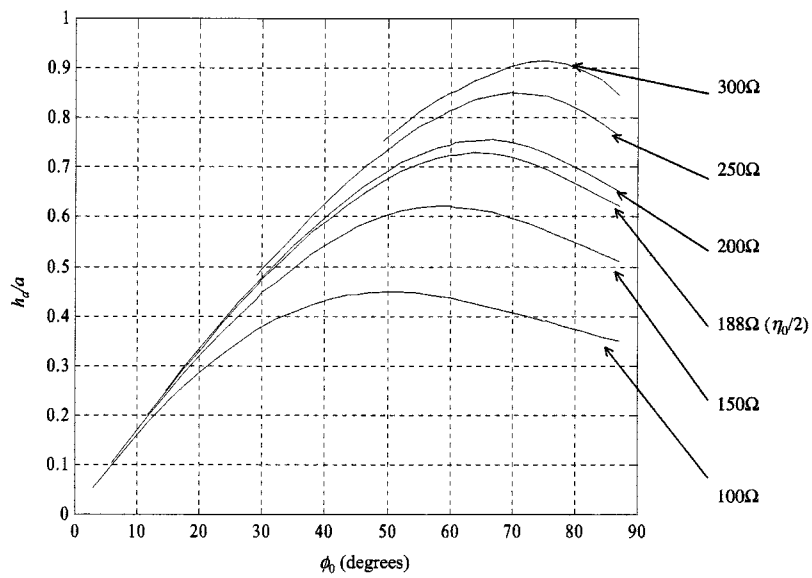

Fig. 6. Normalized aperture height as a function of feed arm angle ϕ_0.

and feed arm angle can be obtained by interpolating between the curves presented in Fig. 5.

B. Aperture Height

Fig. 6 presents the aperture height as a function of ϕ_0 for popular values of the feed impedance. As $b_1 \to a$, $h_a \to a \sin \phi_0$, which is one-half of the mean charge separation for a four-wire transmission line [7]. As $b_1 \to 0$, $h_a \to 0$. The family of curves in Fig. 6 has been fit to a functional form and is tabulated in [18], but once again accurate estimates can be obtained by interpolation between the curves in Fig. 6.

C. Aperture Efficiency

Fig. 7 presents a surface plot of aperture efficiency as a function of b_1/a and ϕ_0. It is clear from Fig. 7 that there is a particular pair of ϕ_0 and b_1/a that produces the maximum aperture

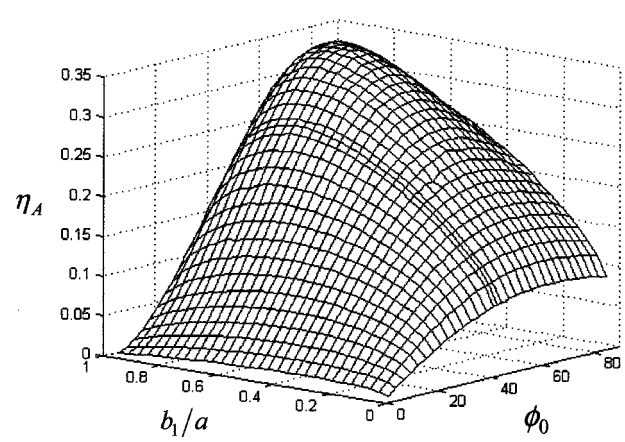

Fig. 7. Mesh plot of aperture efficiency as a function of b_1/a and ϕ_0. There is a clear maximum at $\phi_0 = 70°$ and $b_1/a = 0.84$. The value of f_g at this point is 0.65 (247 Ω in free space).

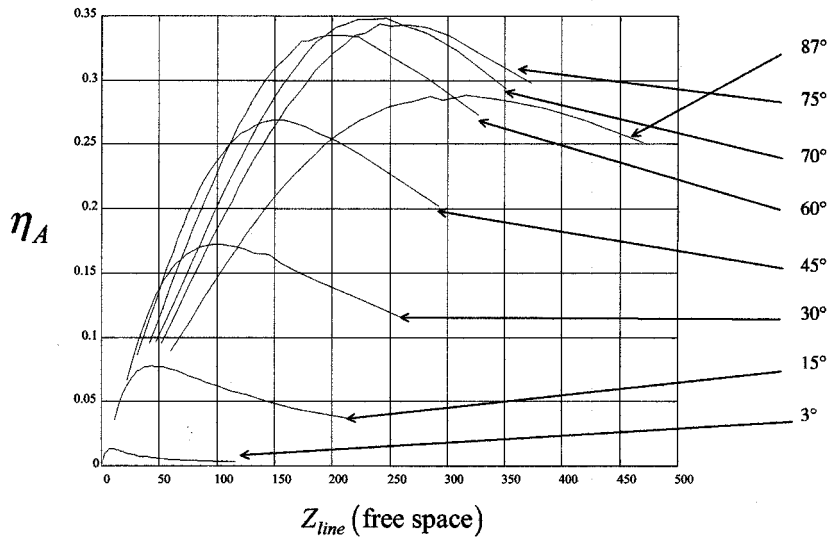

Fig. 8. Plots of aperture efficiency as a function of feed impedance (in free space). As ϕ_0 increases, the curves shift to the right. The graph shows that the optimum feed impedance increases monotonically with ϕ_0.

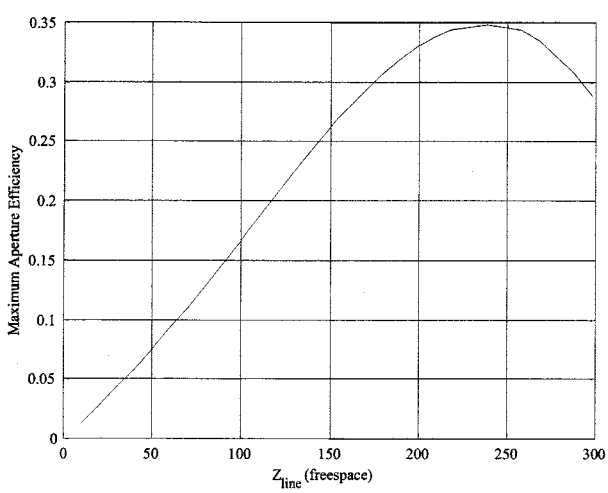

Fig. 9. Optimum aperture efficiency as a function of feed impedance. The peak aperture efficiency is 35% at $Z_{\rm line} = 247\ \Omega$. The optimum angle ϕ_0 for each value of $Z_{\rm line}$ can be obtained from Fig. 10 or (12).

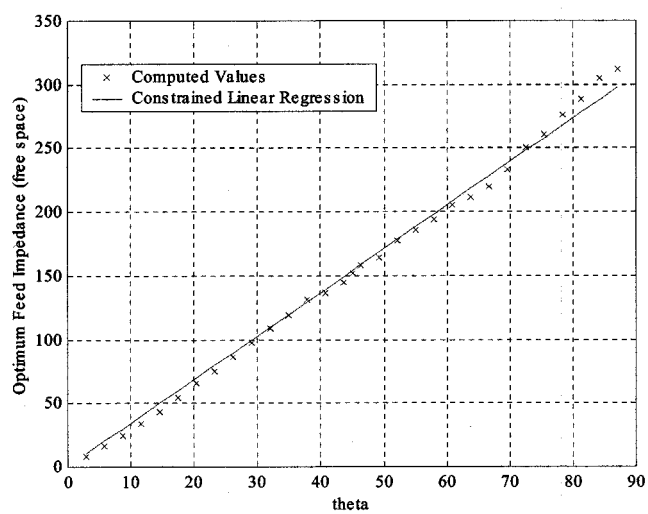

Fig. 10. Optimum feed impedance as a function of ϕ_0. The staircased nature of the data is due to similarities in the progression of the adaptive refinement method and stopping strategies between similar geometries. The linear regression was a slope fit only, as the line was constrained to pass thought the origin. Note that the optimum angle for impedances of 100, 150, 200, and 250 Ω are approximately 30°, 45°, 60°, and 75°, respectively.

efficiency. The maximum value is $\eta_a = 0.35$, and it occurs at $\phi_0 = 70°$, $b_1/a = 0.84$. Fig. 7 shows that $\eta_a \to 0$ as $b_1 \to 0$ and $b_1 \to a$, as demonstrated in [10].

IV. Discussion

The data presented in Figs. 5–7 provide all of the information needed to design an antenna with a particular aperture efficiency, feed impedance, or feed arm angle ϕ_0. However, if the information contained in Figs. 5–7 is combined, curves of η_a versus f_g can be plotted for distinct values of ϕ_0, as is done in Fig. 8.

Analysis of Fig. 8 provides two interesting results. First, for any particular value of feed impedance, there is a unique geometry that provides the optimum aperture efficiency. The curves in Fig. 8 can be used as a design tool to select a particular feed geometry to match the impedance of an individual source. Second, it is clear from the figure that as ϕ_0 increases, the optimum aperture efficiency occurs at higher and higher impedances. The peak value of the aperture efficiency for each ϕ_0 is plotted in Fig. 9, and the feed impedance corresponding to this peak is plotted as a function of ϕ_0 in Fig. 10. The relationship between optimum feed impedance and ϕ_0 appears to be linear, so the data points were fit using a constrained least squares linear regression (setting the intercept to zero). The equation for the line in Fig. 10 is

$$\phi_{0,\rm opt} = 1.9234 \frac{Z_{\rm line}}{120\pi} \tag{12}$$

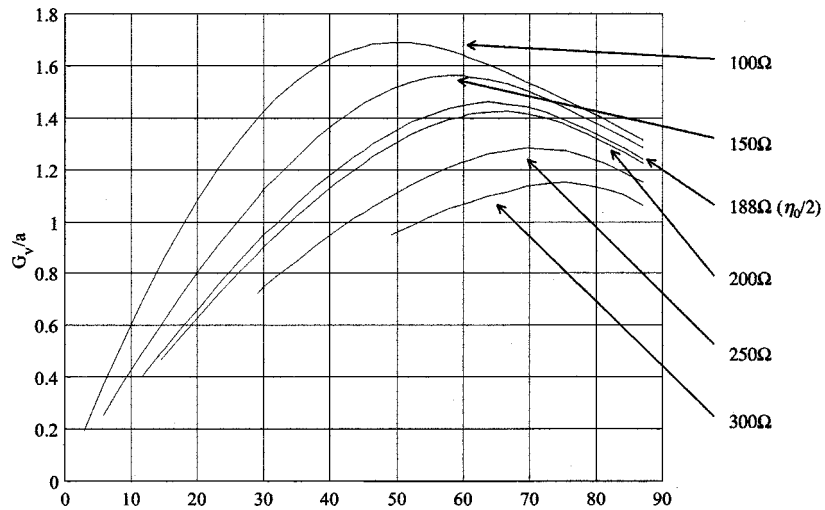

Fig. 11. Voltage normalized gain as a function of feed arm angle for popular values of feed impedance, assuming that the feed line is in free space. The lower the feed impedance, the higher G_v, but this enhancement may be offset by increased feed blockage at lower impedances.

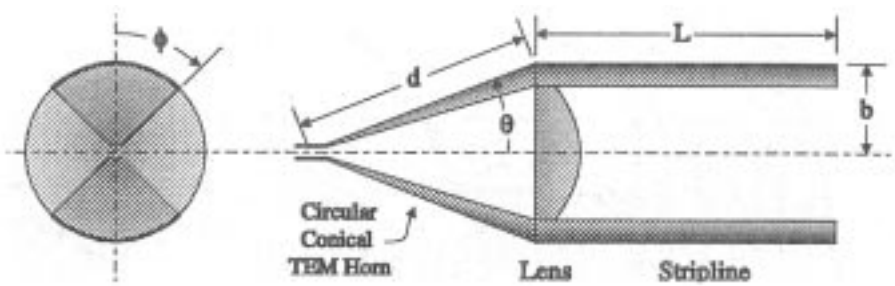

Fig. 12. Circular-conical TEM horn-fed lens IRA. The antenna depicted above is configured with a stripline extension to enhance the late-time response. The 90° section ($\phi = 45°$) has been shown by Liu [20] to be the optimum geometry for self-reciprocal feed structures. The optimum configuration for the four-arm IRA is that that most closely approximates the circular conical IRA.

assuming that the medium is free space. This linear relationship between optimum feed impedance and ϕ_0 was unexpected, and if closed-form expressions for the conformal mapping can be obtained, they might provide some physical understanding of the interaction among feed arm angle, extent of the electrodes, and aperture efficiency. It is worth noting that (12) predicts an optimum impedance of 307 Ω for the case of $\phi_0 = 90°$ when the two pairs of crossed coplanar feeds are at the same location, corresponding to the case of a single pair of coplanar feeds. This geometry was optimized analytically by Farr and Baum in [9] using the parameter G_p. The optimum impedance was found analytically to be 302 Ω, a difference of less than 2% that is attributable to the numerical techniques used in this study.

In this paper, the optimization was considered for the aperture efficiency (or, equivalently, the power normalized gain of [9]). However, for many UWB systems, the quantity that should be maximized is the prompt radiated field, which scales like h_a/f_g, or the voltage normalized gain (G_v) of [9]. As mentioned in the introduction and found in [9], the voltage normalized gain is usually optimized by allowing $f_g \to 0$. Allowing $f_g \to 0$ is impractical for current-flow reasons (since current on the antenna goes like f_g^{-1}), and the wide feed arms needed to obtain low impedances may be expected to significantly enhance feed blockage [19]. For many high-power applications that are limited by dielectric breakdown, the cost of the system scales with input voltage (not input power), so the importance of G_v for maximizing the radiated field should not be overlooked. The value of G_v (normalized to the aperture radius a) is plotted as a function of ϕ_0 in Fig. 11 for several common values of feed impedance.

The results reported here were for the four-arm IRA, but there is nothing preventing a similar analysis of N-arm IRAs. The optimum aperture efficiency for the two-arm IRA can be computed using the results from [9] and is 27%. The optimum aperture efficiency for the four-arm case considered here is 35%. Intuitively, the addition of *nonblocking* feed arms will continue to optimize the aperture efficiency. This is true because additional feeds cause the field distribution in the aperture to be more uniform, hence increasing aperture efficiency. It was shown in [10] that $\eta_A \leq 50\%$ for all self-reciprocal antennas that focus the circle of symmetry, and it was demonstrated in [20] that the circular conical feed structure depicted in Fig. 12 with $\phi = 45°$ has the most uniform field distribution in the aperture. It can therefore be concluded that the optimum four-arm IRA, with $\phi_0 = 70°$, $b_1/a = 0.84$, and $f_g = 0.65$, is the one that most closely approximates the geometry depicted in Fig. 12. Furthermore, if only the *prompt* signal is considered, the addition of more nonblocking feed arms will make a better approximation

to the geometry in Fig. 12, further improving the aperture efficiency. However, the late-time field will be pulled down more rapidly as more feed arms are added even in the absence of feed blockage.

The analysis presented in this paper assumed no feed blockage by the coplanar feed lines. This assumption corresponds to the geometric optics analysis that is typically used for IRAs. The presence of large metallic plates in the aperture might be expected to perturb the aperture distribution, thereby reducing the aperture efficiency below that predicted by the geometric optics analysis. Quantification of the effect of aperture blockage in coplanar-plate fed IRAs is an issue that merits further investigation.

V. Conclusion

The study described in this paper has provided three principle results. First, the entire design space for reflector IRAs fed by crossed coplanar feeds with reflection symmetry has been sampled. Curves are presented in Figs. 5–9 that allow ready prediction of feed impedance, aperture height, and aperture efficiency as a function of the geometric parameters of the antenna. These relationships provide more flexibility in IRA design than what was possible using configurations with known analytic solutions [9]. Second, the data presented in this paper allow the optimization of the aperture efficiency for any value of the geomteric properties. It has been shown that a distinct optimum exists for any feed arm angle ϕ_0 and that an absolute optimum configuration exists at $\phi_0 = 70°$, $b_1/a = 0.84$, and $f_g = 0.65$ (247 Ω in free space). Finally, the results presented in Figs. 8 and 10 show that for any specific value of feed impedance, there is a unique optimum configuration that maximizes aperture efficiency. The curves in those figures cover several common feed impedances, including the 200-Ω case used in many reflector IRAs. The feed arm angle is linearly related to the desired impedance by (12). This is important in that once the input impedance of the antenna is specified, the antenna can be optimized without affecting upstream components of the system by selecting the appropriate values of ϕ_0 and b_1/a presented in this paper.

The methods used in this report are general in that they can be applied to any focused aperture system to calculate feed impedance and aperture height (and hence any of the performance metrics described above). While best suited to the analysis of self-reciprocal apertures, iterative boundary condition methods have been developed that allow computation of open TEM modes [16], [10]. The method can be easily modified to include the effects of aperture blockage in the evaluation of (3), allowing analysis of geometries for the feed arms that are not coplanar plates, including circular-cross-sectioned feed arms, curved plates, or other arbitrary configurations.

Acknowledgment

The author would like to thank C. E. Baum and C. J. Buchenauer for their helpful comments during the writing of this paper.

References

[1] D. V. Giri and C. E. Baum, "Temporal and spectral radiation on boresight of a reflector type of impulse radiating antenna," in *Ultra-Wideband, Short Pulse Electromagnetics*, C. E. Baum, L. Carin, and A. P. Stone, Eds. New York: Plenum, 1997, vol. 3, pp. 65–72.

[2] C. E. Baum and E. G. Farr, "Impulse radiating antennas," in *Ultra Wideband/Short Pulse Electromagnetics*, H. L. Bertoni, C. E. Baum, and L. B. Felson, Eds. New York: Plenum Press, 1993, pp. 139–147.

[3] E. G. Farr, C. E. Baum, and C. J. Buchenauer, "Impulse radiating antenna, part II," in *Ultra-Wideband, Short-Pulse Electromagnetics*. New York: Plenum, 1995, vol. 2, pp. 159–170.

[4] E. G. Farr and C. E. Baum, "Impulse radiating antennas, part III," in *Ultra-Wideband, Short-Pulse Electromagnetics*, C. E. Baum, L. Carin, and A. P. Stone, Eds. New York: Plenum, 1997, vol. 3, pp. 43–56.

[5] ——, *Prepulse Associated with the Feed of an Impulse Radiating Antenna*, C. E. Baum, Ed. Albuquerque, NM: USAF Phillips Lab, Mar. 1992. *Sensor and Simulation Notes* #337.

[6] C. E. Baum, E. G. Farr, and D. V. Giri, "Review of impulse radiating antennas," in *Review of Radio Science*, W. R. Stone, Ed. Oxford, U.K.: Oxford Univ. Press, 1999, ch. 16, pp. 403–439.

[7] C. E. Baum, *Aperture Efficiencies of IRAs*, C. E. Baum, Ed. Albuquerque, NM: USAF Phillips Lab, June 1991. *Sensor and Simulation Notes* #328.

[8] E. G. Farr and C. E. Baum, *Extending the Definitions of Antenna Gain and Radiation Pattern into the Time Domain*, C. E. Baum, Ed. Albuquerque, NM: USAF Phillips Lab, Nov. 1992. *Sensor and Simulation Notes* #350.

[9] ——, *Optimizing the Feed Impedance of Impulse Radiating Antennas Part I: Reflector IRAs*, C. E. Baum, Ed. Albuquerque, NM: USAF Phillips Lab, Jan. 1993. *Sensor and Simulation Notes* #354.

[10] C. J. Buchenauer, J. S. Tyo, and J. S. H. Schoenberg, "Aperture efficiencies of impulse radiating antennas," IEEE Transaction on Antennas and Propagation, Aug. 1999. submitted to (also *Sensor and Simulation Notes* SSN#421, C. E. Baum, Ed., Nov. 1997 (USAF Research Lab., Albuquerque, NM)), to be published.

[11] E. G. Farr, *Optimization of the Feed Impedance of Impulse Radiating Antennas, Part II: TEM Horns and Lens IRAs*. Albuquerque, NM: USAF Phillips Lab., Nov. 1995. *Sensor and Simulation Notes* SSN#384.

[12] E. G. Farr and C. E. Baum, "Radiation from self-reciprocal apertures," in *Electromagnetic Symmetry*, C. E. Baum and H. N. Kritikos, Eds. Bristol, PA: Taylor and Francis, 1995, ch. 5.

[13] C. E. Baum, *Selection of Angles Between Planes of TEM Feed Arms of an IRA*. Albuquerque, NM: USAF Research Lab, Aug. 1998. *Sensor and Simulation Notes* #425.

[14] *Static and Dynamic Electricity*, 3rd ed. Washington, DC: Taylor and Francis, 1989, ch. 4, pp. 63–120.

[15] *Field Theory Handbook*, Springer-Verlag, Berlin, Germany, 1961.

[16] C. J. Buchenaeur, J. S. Tyo, and J. S. H. Schoenberg, "Antennas and electric field sensors for ultra wideband transient measurements: Applications and methods," in *Ultra-Wideband, Short-Pulse Electromagnetics*, C. E. Baum, L. Carin, and A. P. Stone, Eds. New York: Plenum Press, 1997, vol. III, pp. 405–421.

[17] *Handbook of Mathematical Functions*, Dover, New York, 1965.

[18] J. S. Tyo, *Optimization of the Feed Impedance for an Arbitrary Crossed-Feed-Arm Impulse Radiating Antenna*, C. E. Baum, Ed., Nov. 1999. *Sensor and Simulation Notes* #438.

[19] E. G. Farr, , Oct. 1999. Personal Communication.

[20] T. K. Liu, *Impedances and Field Districutions of Curved Parallel-Plate Transmission-Line Simulators*. Albuquerque, NM: USAF Research Lab., Feb. 1973. *Sensor and Simulation Notes* SSN#170.

J. Scott Tyo (S'96–M'97) was born in Germany in 1972. He received the B.S.E., M.S.E., and Ph.D. degrees in electrical engineering from the University of Pennsylvania, Philadelphia, in 1994, 1996, and 1997, respectively.

From 1996 to 1999, he was assigned to the Directed Energy Directorate of the Air Force Research laboratory, Kirtland AFB, NM, where he performed research on generation and radiation of high-power, ultra-wide-band microwave signals. Since 1999, he has been assigned to the Naval Postgraduate School, Monterey, CA, where he is an Assistant Professor in the Electrical and Computer Engineering Department. His research interests involve ultra-wide-band electromagnetics as well as microwave and optical remote sensing.

Capt. Tyo is a member of Tau Beta Pi and Eta Kappa Nu.